AAS 07-129

ADAPTIVE ENTRY NAVIGATION USING INERTIAL MEASUREMENTS

Renato Zanetti * **and Robert H. Bishop**†

Abstract

The application of a multiple model adaptive estimation architecture to entry navigation during the highly dynamic hypersonic pre-parachute deploy phase is investigated. The entry navigation filter design processes inertial measurement unit outputs of acceleration and attitude rates in an extended Kalman filter as external measurements, rather than using the more traditional dead-reckoning approach. The high uncertainty associated with the Martian atmospheric density is addressed with multiple dynamic models comprising a filter bank. The proposed filtering architecture produces state estimates to accuracies comparable to dead-reckoning process, but shows substantial improvement in robustness to uncertainty in the atmosphere.

INTRODUCTION

A reliable navigation system is an essential element of a fully autonomous, closed-loop guidance, navigation, and control (GN&C) system for Mars entry, descent, and landing (EDL). A mission that employs fully autonomous EDL guidance at Mars has not yet flown. The traditional approach to EDL navigation is to employ an algorithm that dead-reckons the inertial measurement unit (IMU) outputs of acceleration and attitude rates, i.e. the IMU measurements are used to propagate the spacecraft state (position, velocity, and attitude). Dead-reckoning is characterized by the absence of an aerodynamic forces model within the navigation algorithm. This is a sensible navigation strategy when the aerodynamic models have large uncertainties at the same time time that the IMU hardware is capable of accurately providing measurements of the non-gravitational accelerations. Fortunately, knowledge of the Mars atmosphere has improved over time thanks to data collected from various successful planetary exploration missions. Nevertheless, the lack of predictability of the atmosphere makes the task of modeling the aerodynamic forces challenging.

Despite the challenges of processing the IMU data in a model-based navigation algorithm, there are valid reasons for considering abandoning the dead-reckoning

*PhD Candidate, Student Member, AIAA.

†Professor of Aerospace Engineering & Engineering Mechanics, Member, AAS, Fellow, AIAA.

approach during the upper atmospheric hypersonic phase of EDL. First, the model-based approach provides the ability to accurately navigate through data drop-outs. Although thought to be an unusual event, IMU data dropouts can lead to large state estimation errors that can be mitigated with a model-based approach. Second, the Kalman filtering approach naturally provides a state estimation covariance that accurately represents the state uncertainty, thereby leading to superior estimation accuracies once other external sensors become available, notably the altimeter after heat shield jettison and parachute deploy. Finally, if a properly configured filter bank is employed in a multiple-model adaptive estimation (MMAE) architecture, changes in the atmosphere can be detected.

The first goal of this investigation is to filter actual IMU measurements from a NASA Mars landing mission. We employ an extended Kalman filter (EKF) for this purpose. Previous works[1] have employed sigma point Kalman filters to accomplish the same goal. The EKF will process actual mission data collected from Mars Exploration Rover (MER) IMUs. It will be shown that the model-based EKF algorithm leads to better results than dead-reckoning. The second goal of this investigation is to expand the single EKF navigation system to a MMAE architecture in order to account for different possible atmospheric conditions. In previously reported investigations, a different MMAE scheme [2] was used to filter simulated data. In this work a new filter selection scheme is developed and used to process actual MER IMU data.

The MMAE is an adaptable estimation technique that consist of a bank of parallel filters. It has been a topic of great interest since Magill's pioneering work [3]. The Magill scheme has been modified to study a variety of problems. The interacting multiple model (IMM) [4] is a MMAE scheme that has received attention in the past years. To avoid the necessity of having a large bank of filters to implement every possible parameter realization, the concept of moving bank was introduced [5]. Methods to enhance the MMAE performance were investigated [6], and conditions for the effective steady-state performance were studied [7]. The MMAE techniques were successfully used for space structures control [8], and actuator-sensor failure detection in various situations, for example on the F-16 [9]. Other applications are tracking maneuvering targets [10], and estimation in presence of switching coefficients [11].

Together with the filter bank, the MMAE has an hypothesis algorithm that weights each filter in the bank. In the Magill scheme case, the weight is given by the conditional probability and is used to combine the state estimates into a single optimal estimated state. Other possible weighting methods exist, including the single layer gating network [12, 13, 14, 15]. The gating network approach is followed here because it is a "winner take all" strategy consistent with our objective of determining the filter producing the "best" state estimate. Each filter in the bank represents a different realization of the atmosphere (e.g., one filter represent nominal expected density, another represents possible high

density conditions, and so forth). The filter in the bank assigned the highest weight by the gating network indirectly indicates the atmospheric conditions.

Mars EDL Scenario

The EDL phase is one of the most challenging phases of a planetary lander mission. The EDL begins at entry interface (EI), the time when the spacecraft first encounters the sensible atmosphere and switches from the orbit phase to the EDL phase. In orbit, the spacecraft is mainly tracked by Earth-based resources, such as the Deep Space Network. During EDL, the spacecraft are autonomous and must navigate using on-board resources. Shortly after EI, the IMUs begin providing measurements of all nongravitational accelerations (i.e., those to due aerodynamic forces). The spacecraft makes a hypersonic/supersonic descent during which only on-board IMUs, and possibly atmospheric measurements (such as stagnation point pressure), are available. The spacecraft is contained within its aeroshell. On future missions requiring precision landing, it is during this upper atmospheric phase that the guidance will be active. For Apollo, the GN&C system modulated the aerodynamic lift direction by banking the capsule during the time in the Earth's atmosphere. Future GN&C algorithms for planetary missions may also modulate the angle of attack—our proposed navigation structure remains applicable in this case.

At about Mach 2+ (or an altitude of approximately 10 km), one or several parachutes are deployed and the aeroshell is jettisoned, allowing ranging instruments on-board to provide a measurement of the proximity to the ground. At this point, more advanced sensors can also map the terrain. Once the heat shield is jettisoned and the altimeter and velocimeter, now exposed to the external environment, provide measurements to the navigation algorithm, the spacecraft is on the parachute and cannot be actively guided using lift modulation. During this phase of EDL, the navigation uncertainty is significantly reduced, but guidance cannot compensate for any existing state errors. Unless there is an active parachute steering control or there is a decision made to fire the engines on the chute, this is not an active guidance phase.

In the last hundreds of meters above the surface, the parachute is jettisoned and the spacecraft lands on its own power. Once the hazard avoidance sensor is available, guidance can actively be utilized to maneuver the vehicle. By this time there is not much ability to make large excursions to hit a pinpoint landing. In the case of MER, a landing bag system was deployed which resulted in a significant bouncing at the final phase. MER did not use active guidance–it was not a precision targeted landing. Even though our interest is in enabling precision landings, the MER IMU data will be used in this investigation. The available IMU data represents an outstanding data set upon which to test the proposed model-based EKF and MMAE architecture.

EXTENDED KALMAN FILTER

Given that the IMU the only available sensor during upper atmospheric hypersonic/supersonic phase of the EDL, the dead-reckoning approach uses only state integration with given initial conditions. The accuracy of the initial conditions depend on the quality of the spacecraft tracking prior to EI. In the terminology of Kalman filtering, dead-reckoning represents state propagation only without any state updates. During the state propagation, the accuracy of the estimate degrades due to random and systematic errors in the IMU. Dependent on the accuracy of the IMU, the state estimation error covariance necessarily increases. Using a model-based EKF approach, the goal is to improve the state estimate sufficiently during the state update to compensate for atmospheric and IMU modeling errors. It is expected that only the estimate of velocity will be substantially improved over time, because position is very poorly observable from aerodynamic acceleration measurements. As the velocity estimation error decreases with time, filtering the IMU data will lead to better overall navigation than with dead-reckoning.

In the remainder of this section, various aspects of the extended Kalman filter are presented. It will be shown that is possible to improve state knowledge using EKF processing IMU data. The EKF also serves as the main computational building block of the MMAE. Every filter in the MMAE filter bank will be of the form presented in this section, the only difference will be in the realization of the atmospheric model. The gating network selection algorithm employed in the MMAE is also presented.

Filter Model

The translation and attitude motion of the spacecraft are modeled via

$$\begin{aligned}\dot{\mathbf{r}} &= \mathbf{v} \\ \dot{\mathbf{v}} &= \mathbf{g}(\mathbf{r}) + \mathbf{a}(\mathbf{r}, \mathbf{v}) + \mathbf{w}_p \\ \dot{\overline{\mathbf{q}}} &= \frac{1}{2}\boldsymbol{\Omega}(\boldsymbol{\omega})\overline{\mathbf{q}},\end{aligned}$$

where $\mathbf{g}$ is the gravitation acceleration, $\mathbf{a}$ is the nongravitational acceleration. All translational quantities are expressed in the inertial frame I, and the angular velocity $\boldsymbol{\omega}$ is expressed in the body frame B. Under standard Kalman filter assumptions, the disturbance $\mathbf{w}_p$ is assumed to be zero-mean, white noise process. The EKF propagation equations are given by

$$\begin{aligned}\dot{\widehat{\mathbf{r}}} &= \widehat{\mathbf{v}} \\ \dot{\widehat{\mathbf{v}}} &= \mathbf{g}(\widehat{\mathbf{r}}) + \mathbf{a}(\widehat{\mathbf{r}}, \widehat{\mathbf{v}}) \\ \dot{\widehat{\overline{\mathbf{q}}}} &= \frac{1}{2}\boldsymbol{\Omega}(\boldsymbol{\omega}_m)\widehat{\overline{\mathbf{q}}},\end{aligned}$$

where $\boldsymbol{\omega}_m$ is the gyro measurement (assumed to be compensated for biases and misalignments). Therefore, the IMU gyro measurement is modeled as

$$\boldsymbol{\omega}_m = \boldsymbol{\omega} + \mathbf{w}_g,$$

where $\mathbf{w}_g$ is zero-mean white noise process.

The estimation error is defined with the multiplicative quaternion formulation

$$\mathbf{e} \triangleq \begin{bmatrix} (\mathbf{r} - \widehat{\mathbf{r}})^{\mathrm{T}} & (\mathbf{v} - \widehat{\mathbf{v}})^{\mathrm{T}} & \delta\mathbf{q}_v^{\mathrm{T}} \end{bmatrix}^{\mathrm{T}},$$

where $\mathbf{q}_v$ is the vector component of the quaternion $\delta\overline{\mathbf{q}}$ defined as

$$\delta\overline{\mathbf{q}} \triangleq \overline{\mathbf{q}} \otimes \widehat{\overline{\mathbf{q}}}^{-1}.$$

To first-order, the evolution of the estimation error is given by

$$\dot{\mathbf{e}} = \frac{d}{dt}\begin{bmatrix} \mathbf{e}_r \\ \mathbf{e}_v \\ \delta\mathbf{q}_v \end{bmatrix} = \begin{bmatrix} \mathbf{e}_v \\ \mathbf{G}(\widehat{\mathbf{r}})\mathbf{e}_r + \mathbf{A}_r\mathbf{e}_r + \mathbf{A}_v\mathbf{e}_v + \mathbf{w}_p \\ -\boldsymbol{\omega}_m \times \delta\mathbf{q}_v - 0.5\,\mathbf{w}_g \end{bmatrix}, \tag{1}$$

where

$$\mathbf{A}_r := \left.\frac{\partial \mathbf{a}}{\partial \mathbf{r}}\right|_{r=\hat{r},v=\hat{v}} \quad \text{and} \quad \mathbf{A}_v := \left.\frac{\partial \mathbf{a}}{\partial \mathbf{v}}\right|_{r=\hat{r},v=\hat{v}}.$$

The approach taken here in the EKF development is to update the position and velocity estimates with the accelerometer measurement, and to dead-reckon the attitude estimate. The reasoning is as follows. Once through the upper atmosphere hypersonice/supersonic phase, other EDL sensors (such as the altimeter and velocimeter) will be available to provide information about translational states. Those measurements can naturally be fused together with the accelerometer measurements within the EKF. On the other hand, it is assumed that there are no other attitude sensors available post-parachute deploy, hence the gyro is the only sensor capable of providing attitude information. There is no tangible benefit to updating the attitude estimate with the gyro data unless accompanied by an attitude dynamics model of sufficient complexity to capture the rotational motion of the spacecraft. The additional complexity of the navigation algorithm due to the attitude dynamics model was deemed to be too great for the potential benefit. If an external attitude sensor should in fact become available, then this issue would necessarily be re-visited.

The model for the aerodynamic acceleration expressed in the inertial frame is given by

$$\mathbf{a} = -\frac{C_D S}{2m}\rho\|\mathbf{v}_{rel}\|\mathbf{v}_{rel}.$$

The parameters C_D, S, and m are assumed to be known. The spacecraft velocity relative to Mars atmosphere is denoted by $\mathbf{v}_{rel}$. The atmospheric model is a modified exponential

$$\rho = \rho_1 \exp\{-\beta h + \gamma\cos(\omega_\rho h) + \delta\sin(\omega_\rho h)\}, \tag{2}$$

where h is the altitude. Eq. (2) employs the coefficients of the COSPAR model, which employs data from Viking 1 and Mariner missions. The specific values of ρ_1, β, γ, ω_ρ, and δ are different for each EKF in the MMAE filter bank.

IMU Measurements

The measurements used are the IMU data collected during the MER EDL at a frequency of 8 Hertz. The IMU measurements represent the spacecraft change in velocity, $\Delta\mathbf{v}_m$, and change in angle, $\Delta\boldsymbol{\theta}_m$, (corrected for biases and misalignments) since the last IMU measurement. These $\Delta\mathbf{v}_m$ and $\Delta\boldsymbol{\theta}_m$ are divided by the time interval to obtain the measured acceleration, $\mathbf{a}_m^C$, and angular velocity, $\boldsymbol{\omega}_m$. The accelerometer measurement expressed in the IMU case frame $\mathbf{a}_m^C$ is rotated into the body frame through a known constant rotation matrix

$$\mathbf{a}_m^B = \mathbf{T}_C^B \mathbf{a}_m^C.$$

Measurement Model

The accelerometer measurement has two components: (i) the change in velocity due to nongravitational accelerations, and (ii) the change in velocity due to the offset between the center of mass and the accelerometer location, given by

$$\widehat{\mathbf{a}}_{offset} \simeq \boldsymbol{\omega}_m \times \boldsymbol{\omega}_m \times \mathbf{r}_{offset}.$$

The estimated measurement expressed in the body frame is

$$\widehat{\mathbf{a}}^B = \mathbf{T}^{\mathrm{T}}(\widehat{\mathbf{q}})\widehat{\mathbf{a}} + \widehat{\mathbf{a}}_{offset},$$

The residual $\boldsymbol{\epsilon}$ used to update position and velocity is given by

$$\boldsymbol{\epsilon} = \mathbf{a}_m^B - \widehat{\mathbf{a}}^B.$$

Simulation Results

Simulations show that filtering leads to a more accurate state estimate than dead-reckoning. Figure 1 shows the comparison between the EKF state estimates and the dead-reckoning. Every run is preformed with the same set of IMU data from the MER mission. The error history is obtained comparing a JPL-provided best estimated trajectory (BET) to the EKF state estimate. Each run differs in the initial condition generated with a zero-mean, normal distribution whose covariance is diagonal and has standard deviation of 1000m in each position axes, 100m/s in each velocity axes, 3° in attitude, and mean equal to the initial state of the BET.

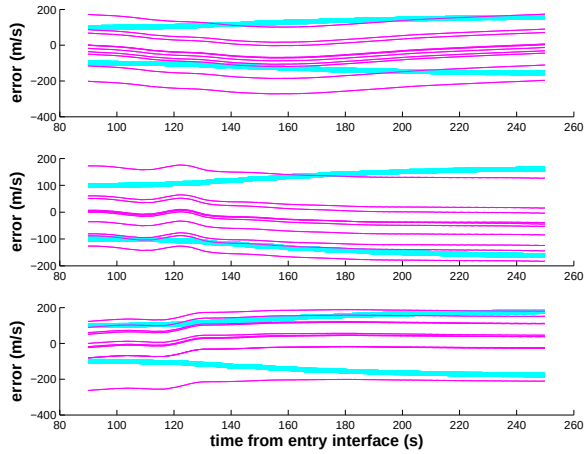

(a) Dead-Reckoning

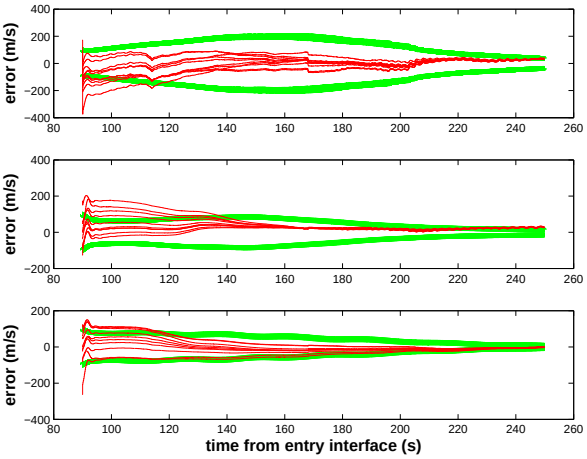

(b) Filtering

Figure 1: Comparison of dead-Reckoning and EKF filtering approach. Ten runs varying the initial conditions and using the same set of MER IMU measurements. The thick line is the standard deviation.

HIERARCHICAL GATING NETWORK

The MMAE scheme employed here is a modified version of that of Chaer et al[14, 15]. Figure 2 show the structure of hierarchical gating network.

A bank of filters with different values of the unknown parameter $\boldsymbol{\alpha}$ is implemented. In our investigations, $\boldsymbol{\alpha}$ represents the various parameters of the

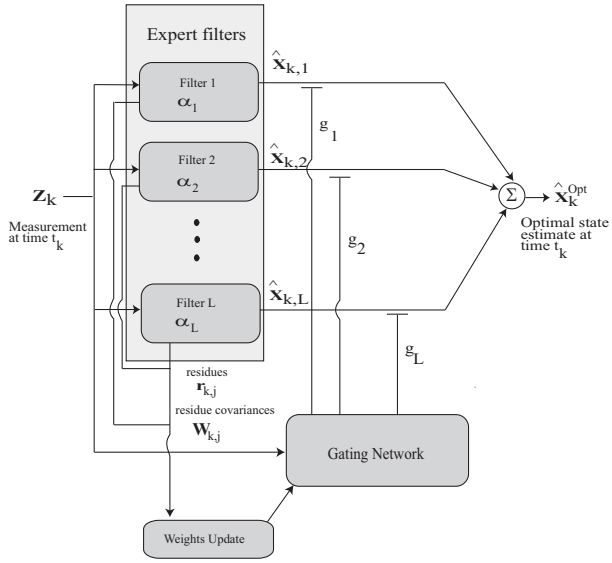

Figure 2: The hierarchical gating network architecture.

COSPAR atmospheric density model. The gating network has to assign a gain g_i to each filter. The gain is interpreted as the filter probability to be the best performing filter in the bank. Let L be the number of filters. To be interpreted as a probability g_i has to satisfy the following characteristics:

$$\begin{gathered} 0 \leq g_i \leq 1, \quad \forall i = 1, 2, ..., L \\ \sum_{i=1}^{L} g_i = 1 \end{gathered} \tag{3}$$

The "max" function assigns 1 to the maximum value between the arguments and zero to the other values. Since the max function is not differentiable, the softmax function

$$g_i = \frac{e^{u_i}}{\Sigma_{i=1}^{L} e^{u_i}} \tag{4}$$

is used instead of the max function. The probability of the entire bank is

$$f(\mathbf{z}_k) = \sum_{i=1}^{L} f(\mathbf{z}_k \mid \boldsymbol{\alpha}_i) P(\boldsymbol{\alpha}_i) = \sum_{i=1}^{L} f(\mathbf{z}_k \mid \boldsymbol{\alpha}_i) g_i, \tag{5}$$

where $P(\cdot)$ denotes probability. The goal is to maximize the probability of the bank. In order to maximize this probability density, it is easier to work with the natural logarithm of $f(\mathbf{z}_k)$, or

$$l \triangleq \ln f(\mathbf{z}_k) = \ln \sum_{i=1}^{L} f(\mathbf{z}_k \mid \boldsymbol{\alpha}_i) e^{u_i} - \ln \sum_{i=1}^{L} e^{u_i}.$$

Taking the derivative of l with respect to u_i yields

$$\frac{\partial l}{\partial u_i} = h_i - g_i, \tag{6}$$

where

$$h_i = P(\boldsymbol{\alpha}_i \mid \mathbf{z}_k) = \frac{f(\mathbf{z}_k \mid \boldsymbol{\alpha}_i) g_i}{f(\mathbf{z}_k)}.$$

Eq. (6) shows the direction of maximum growth of the function l. The update is accomplished via

$$u_i \leftarrow u_i + \eta \frac{\partial l}{\partial u_i} \tag{7}$$

where η is a learning rate parameter. The gating network gains can now be computed with Eq. (4). The scalar u_i can be interpreted as a measure of how likely the i^{th} filter is to be the best performing filter within the bank. The higher the value of u_i, the higher the likelihood that it is the best performing filter. Notice that u_i cannot be interpreted as a probability since $u_i \in \Re$. Eq. (7) can be rewritten as

$$u_i \leftarrow u_i + \eta \left[P(\boldsymbol{\alpha}_i \mid \mathbf{z}_k) - P(\boldsymbol{\alpha}_i) \right]$$

which is intuitive in the following sense: the updated u_i starts from the old value, increases if the probability associated with the last measurement is larger than the old probability, decreases otherwise. The larger the learning rate parameter, the larger the current measurements are weighted. For $\eta = 0$ the gains do not update, for $\eta \to \infty$ the filter with higher probability after measurement $\mathbf{z}_k$ will be given probability one, all others will be given probability zero.

Once the filter weights are computed, the state estimate can be chosen to be the state estimate associated with the winning filter, or it can be a weighted average of the L filters in the bank. In the latter case, the estimated state is given by

$$\widehat{\mathbf{x}} = \sum_{i=1}^{L} g_i \widehat{\mathbf{x}}_i. \tag{8}$$

The estimation error associated with the weighted state estimate is

$$\mathbf{e} = \sum_{i=1}^{L} g_i \left(\widehat{\mathbf{x}}_i - \mathbf{x}_i \right) = \sum_{i=1}^{L} g_i \, \mathbf{e}_i, \tag{9}$$

and the estimation error covariance is

$$\mathbf{P} = \mathrm{E}\left\{ \mathbf{e} \cdot \mathbf{e}^{\mathrm{T}} \right\} = \sum_{i=1}^{L} \sum_{j=1}^{L} g_i g_j \, \mathrm{E}\left\{ \mathbf{e}_i \cdot \mathbf{e}_j^{\mathrm{T}} \right\} = \sum_{i=1}^{L} \sum_{j=1}^{L} g_i g_j \mathbf{P}_{ij} \tag{10}$$

where $\mathbf{P}_{ii}$ is the autocovariance of the i^{th} filter, and $\mathbf{P}_{ij},\ i \neq j$ is the crosscovariance between filters i and j. Recall that

$$\mathbf{e}_i^{+} \simeq \mathbf{e}_i^{-} + \mathbf{K}_i \mathbf{H}_i \mathbf{e}_i^{-} + \mathbf{K}_i \mathbf{w}_a, \tag{11}$$

where $\mathbf{w}_a$ is the accelerometer noise which is a common quantity for all filters in the bank. Then it follows that

$$\mathbf{P}_{ij}^{+} = (\mathbf{I} - \mathbf{K}_i\mathbf{H}_i)\mathbf{P}_{ij}^{-}(\mathbf{I} - \mathbf{K}_j\mathbf{H}_j)^{\mathrm{T}} + \mathbf{K}_i\mathbf{R}\mathbf{K}_j^{\mathrm{T}} \tag{12}$$

where $\mathbf{R}$ is the measurement noise autocovariance, which is also the crosscovariance because the filters share the sensors.

Simulation Results

The algorithm described in the previous section was tested with the MER IMU measurements. The bank was composed of three filters, a filter with the nominal COSPAR air density model, a "high" filter with air density 10% higher than nominal, and a "low" filter with air density 10% lower. Figure 3 shows the evolution of the gains in the bank, Figure 4 shows the total estimation error in position and velocity.

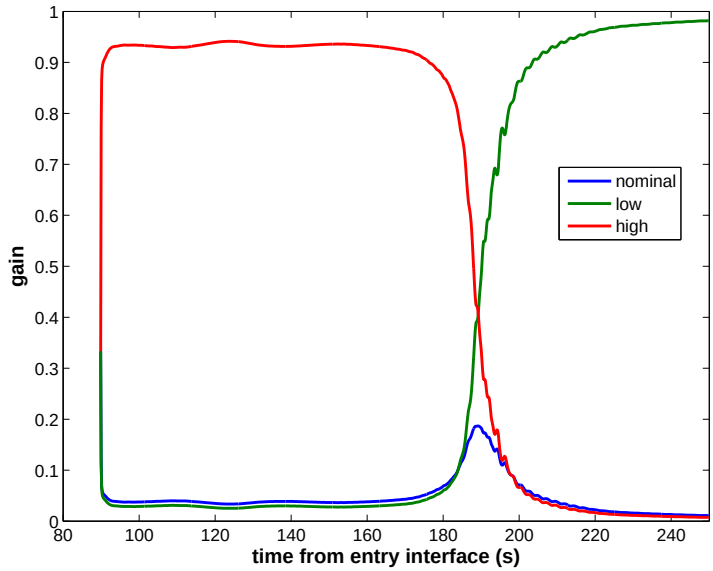

Figure 3: Gain evolution.

In Figure 3, the gain associated with the filter modeling a "high" density situation is assigned the highest weight during the initial 180s, then a switch occurs and the filter modeling a "low" density situation is assigned the highest weight. Correspondingly, in Figure 4 the position and velocity errors are smallest for the filter modeling the "high" density during the first 180s. After about 200s, the filter modeling the 'low" density produces the smallest estimation errors. This shows that the gating network is capable of correctly selecting the best

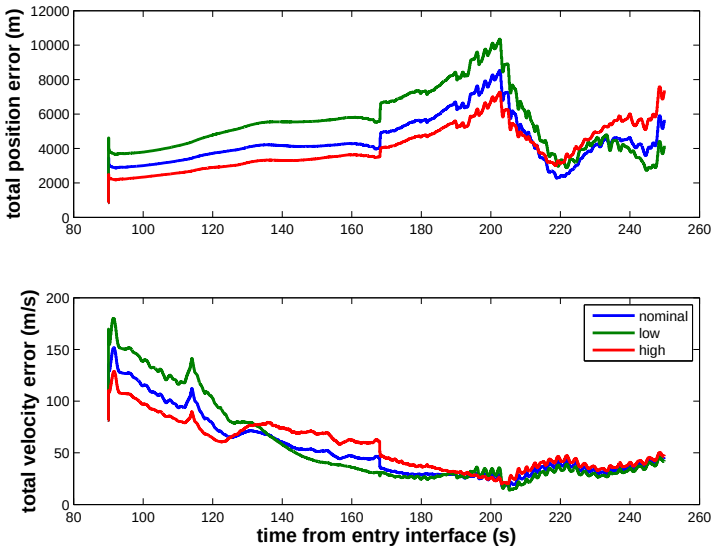

Figure 4: Total position and velocity errors of the three filters in the bank.

filter among the ones implemented in the filter bank.

These results are only indicative of the possibilities of using an EKF for processing the IMU data coupled with the MMAE architecture. This is not an exhaustive investigation, hence no general statements about the MER mission or the atmosphere encountered during the MER EDL should be made. First, the BET provided by JPL was, in fact, not a final BET (that work is still underway), so that the state estimation errors shown in Figures 1 and 4 may not reflect the actual estimation errors. Second, and more importantly, the atmospherice density model used in the analysis (based on the COSPAR data) is likely not of sufficient complexity to accurately reflect the expected density variations at Mars.

CONCLUSIONS

A modification of an existing multiple model adaptive estimator has been successfully implemented for Mars EDL state estimation. It was shown that real flight IMU measurements can be processed as an external measurement in a model-based extended Kalman filter. Filtering the IMU measurements leads to a more accurate state estimate than the dead-reckoning approach.

ACKNOWLEDGMENTS

This work was supported by the NASA Mars Technology Program, Advanced Entry, Descent, and Landing Task, Jet Propulsion Laboratory, California Institute of Technology, Project No. 1263403. Special thanks to Martin Heyne at The University of Texas at Austin.

REFERENCES

[1] M. Heyne, and R. H. Bishop, "Spacecraft Entry Navigation Using Sigma Point Kalman Filtering," *Position, Location and Navigation Symposium*, IEEE and Institute of Navigation, Coronado, CA, 2006.

[2] O. Dubois-Matra, and R. H. Bishop, "Multi-model Navigation with Gating Networks for Mars Entry Precision Landing," *AIAA Atmospheric Flight Mechanics Conference*, Providence RI, August 2004.

[3] D. T. Magill, "Optimal adaptive estimation of sampled stochastic processes," *IEEE Transactions on Systems, Man and Cybernetics*, vol. AC-10, pp. 434–439, October 1965.

[4] H. A. P. Blom, "An efficient filter for abruptly changing systems," in *Proceedings 23rd IEEE Conference on Decision and Control*, 1984.

[5] P. S. Maybeck and K. P. Hentz, "Investigation of moving-bank multiple model adaptive algorithma," *AIAA Journal of Guidance, Control, and Dynamics*, vol. 10, no. 1, pp. 90–96, January-February 1978.

[6] P. S. Maybeck and P. D. Hanlon, "Performance enhancement of a multiple model adaptive estimator," in *Proceedings of the 32nd Conference on Decision and Control*, 1993.

[7] M. J. Caputi, "A necessary condition for effective performance of the multiple model adaptive estimator," *IEEE Transactions on Aerospace and Electronic Systems*, vol. 31, no. 3, pp. 1132–1138, July 1995.

[8] J. A. Gustafson and P. S. Mayback, "Flexible spacestructures control via moving-bank multiple model algorithms," *IEEE Transactions on Aerospace and Electronic Systems*, vol. 30, no. 3, pp. 750–, July 1994.

[9] P. Eide and P. Maybeck, "An mmae failure detection system for the f-16," *IEEE Transactions on Aerospace and Electronic Systems*, vol. 32, no. 3, pp. 1125–1136, July 1996.

[10] W. D. Blair and Y. Bar-Shalom, "Traking maneuvering targets with multiple sensors: Does more data always mean better estimates?" *IEEE Transactions on Aerospace and Electronic Systems*, vol. 32, no. 1, pp. 450–456, January 1996.

[11] H. A. P. Blom and Y. Bar-Shalom, "The interacting multiple model algorithm for systems with markovian switching coefficients," *IEEE Transactions on Automatic Control*, vol. 33, no. 8, pp. 780–783, August 1988.

[12] R. A. Jacobs and M. I. Jordan, "A competitive modular connectionist architecture," *Advances in Neural Information Processing Systems 3*, R. P. Lippman et al., Eds. San Mateo, CA: Morgan Kaufmann, 1991, pp. 767773.

[13] ——, "Hierarchies of adaptive experts," *Advances in Neural Information Processing Systems 4*, J. E. Moody et al., Eds. San Mateo, CA: Morgan Kaufmann, 1992, pp. 985992, 1992.

[14] W. S. Chaer, R. H. Bishop, and J. Ghosh, "A mixture-of-experts framework for adaptive kalman filtering," *IEEE Transactions on Systems, Man and Cybernetics-Part B: Cybernetics*, vol. 27, no. 3, pp. 452–464, 1997.

[15] ——, "Hierarchical adaptive kalman filtering for interplanetary orbit determination," *IEEE Transactions on Aerospace and Electronic Systems*, vol. 34, no. 3, pp. 883–896, July 1998.